



IMPACT OF SOIL FREEZING ON THE CONTINENTAL-SCALE SEASONAL CYCLE SIMULATED BY A GENERAL CIRCULATION MODEL

Kumiko Takata¹, Masahide Kimoto²

1. Domestic Research Fellow, National Institute of Environmental Studies, Onogawa, Tsukuba 305, Japan
e-mail: takata@nies.go.jp

2. Center for Climate System Research, University of Tokyo, Komaba, Meguro, Tokyo 153, Japan
e-mail: kimoto@ccsr.u-tokyo.ac.jp

Abstract

Frozen ground can have great effects on energy and water cycles at a continental scale because of its large coverage, large thermal inertia due to latent heat of fusion, and impermeability. This paper assesses thermal and hydrological impacts of soil freezing, from an interactive point of view, using an atmospheric general circulation model with a multi-layer soil submodel. Experiments are conducted with and without the freezing process and the difference between them is examined.

Inclusion of the freezing process leads to lower surface soil moisture in summer in the frozen-ground region. It results in higher surface temperatures, leading to the stronger water vapor fluxes and larger precipitation associated with the stronger summer monsoon. In this way the climatic effects of frozen ground are found not only in the high latitudes but also in the lower latitudes.

List of symbols

c : volumetric heat capacity of soil
 C_E : bulk coefficient for evaporation
 C_H : bulk coefficient for sensible heat flux
 C_M : bulk coefficient for momentum flux
 c_p : specific heat of air at constant pressure
 D : diffusion coefficient of soil moisture
 F_T : surface sensible heat flux
 F_q : surface latent heat flux
 F_v : surface momentum flux
 L_i : latent heat of fusion
 q_a : surface air specific humidity
 q_s^* : saturation specific humidity at T_a
 T : soil temperature
 T_a : surface air temperature
 T_s : ground surface temperature
 t : time
 v_a : surface wind vector
 W : soil water content
 W_{total} : total water holding capacity
 W_{wilt} : wilting level
 z : vertical coordinate of soil
 β : evaporation efficiency
 k : soil thermal conductivity
 θ_i : volumetric ice content

θ_s : saturation volumetric water content
 θ_w : volumetric soil moisture content
 ρ : air density
 ρ_i : ice density
 ρ_w : water density

Introduction

The importance of land surface processes in climate systems has been widely recognized. Regarding the effects of soil moisture, a large number of studies have been carried out (e.g., Delworth and Manabe, 1989). Frozen ground is another phase of soil moisture. It is spread extensively in high latitude terrestrial areas (Dostovalov and Kudryavtsev, 1967), and has large thermal inertia due to the latent heat of freezing and melting. It also forms an impermeable layer when saturated. It could, therefore, have significant effects on energy and water cycles at continental scale.

In situ relations between permafrost and meteorological conditions have been well examined using observational station data (e.g., Romanovsky and Osterkamp, 1995). In addition, some attempts have been made to estimate changes in permafrost in response to climatic changes, such as global warming, using a land-surface model (e.g., Waelbroeck, 1993). These studies, however, treat only the one-way response of soil to an atmospheric forcing.

This paper assesses the climatic effects of frozen ground, from an interactive point of view, using an atmospheric general circulation model (AGCM). Major attention is paid to the climatological seasonal cycle at a continental scale.

The model

An atmospheric general circulation model (CCSR/NIES AGCM, Numaguti et al., 1995) is used with a multi-layer soil model. The AGCM simulates the global atmospheric circulation with incident solar radiation as an energy input and with real orography as a lower boundary condition. It includes a radiation scheme (Nakajima et al., 1995), a cumulus cloud development scheme simplified from Arakawa and Schubert (1974), prognostics of cloud water (Le Treut et al., 1991), a turbulence closure scheme (Mellor and Yamada, 1982) and a parameterization for orographic gravity wave drag (McFarlane, 1987). In this study, horizontal resolution is about 600 km (T21), vertical resolution is 20 layers between the surface and 10 hPa, and sea surface temperature is prescribed at climatological values including a seasonal cycle.

The soil model is 2 m in depth with three layers (0-5, 5-40, 40-200 cm). Soil temperature, T , is predicted using a thermal conduction equation,

$$\frac{\partial cT}{\partial t} = \frac{\partial}{\partial z} \left(k \frac{\partial T}{\partial z} \right) + L_i \frac{\rho_w}{\rho_i} \frac{\partial \theta_i}{\partial t} \quad [1]$$

where c is volumetric heat capacity of soil, k is thermal conductivity, L_i is latent heat of fusion, ρ_i is ice density, ρ_w is water density and θ_i is volumetric ice content.

Changes in volumetric soil moisture, θ_w , are calculated by a diffusion equation,

$$\frac{\partial \theta_w}{\partial t} = \frac{\partial}{\partial z} \left(D \frac{\partial \theta_w}{\partial z} \right) \quad [2]$$

where D is soil moisture diffusivity. c , k and D are given uniform values, globally. Soil moisture flux is assumed to be zero when a part of soil moisture in an adjacent layer is frozen. Excess of soil moisture in each layer beyond saturation is extracted from the soil as runoff and removed from the system.

Phase change process is modeled by an isothermal approach, that is, during a computation time step, a freezing or thawing layer is considered to be isothermal and has a temperature equal to the freezing point. Fully frozen layers have a temperature below the freezing point.

Surface fluxes are estimated by bulk formulae (Louis, 1979),

$$F_v = -\rho C_M |v_a| v_a \quad [3a]$$

$$F_T = \rho c_p C_H |v_a| (T_s - T_a) \quad [3b]$$

$$F_q = \beta \rho C_E |v_a| (q^*_s - q_a) \quad [3c]$$

where $F_{v,T,E}$ are surface fluxes of momentum, sensible and latent heat, $C_{M,H,E}$ are bulk coefficients, ρ is air density, c_p is specific heat of air at constant pressure, v_a is wind vector, $T_{s,a}$ are surface and air temperatures, q_a is atmospheric specific humidity and q^*_s is saturation specific humidity at T_s . The evaporation efficiency β is estimated from soil moisture θ_w as,

$$\beta = \min(\theta_w / 0.75\theta_s, 1) \quad [4]$$

where $\min(a,b)$ denotes a function to take a smaller value between a and b , and θ_s is saturation volumetric water content. Evaporation is assumed to be equal to potential evaporation when θ_w is greater than 0.75 of θ_s (Manabe, 1969).

Experiments

Two types of experiments were performed: with (F run) and without (N run) the freezing and melting processes of soil moisture. In N run, soil moisture exists as a supercooled water when soil temperatures are below the freezing point. Switching off the freezing process has, therefore, two effects: one is that latent heat of freezing and melting is ignored, and the other is that impermeability of frozen ground is ignored.

It takes 10 years and 5 years respectively for the model to equilibrate with and without the freezing process. The model is integrated for a further 20 years, and the mean of the last 20 years is used to calculate a climatological seasonal cycle. The difference of the climatology between F run and N run (F-N) is used to examine impacts of the freezing process, employing 10 day-mean data.

Results and discussion

The calculated global distribution of seasonally frozen ground (Figure 1a) is defined as the regions where the annual maximum of frozen ratio, $\theta_i/(\theta_i+\theta_w)$, in the uppermost layer is greater than 1 (for 10 day mean),

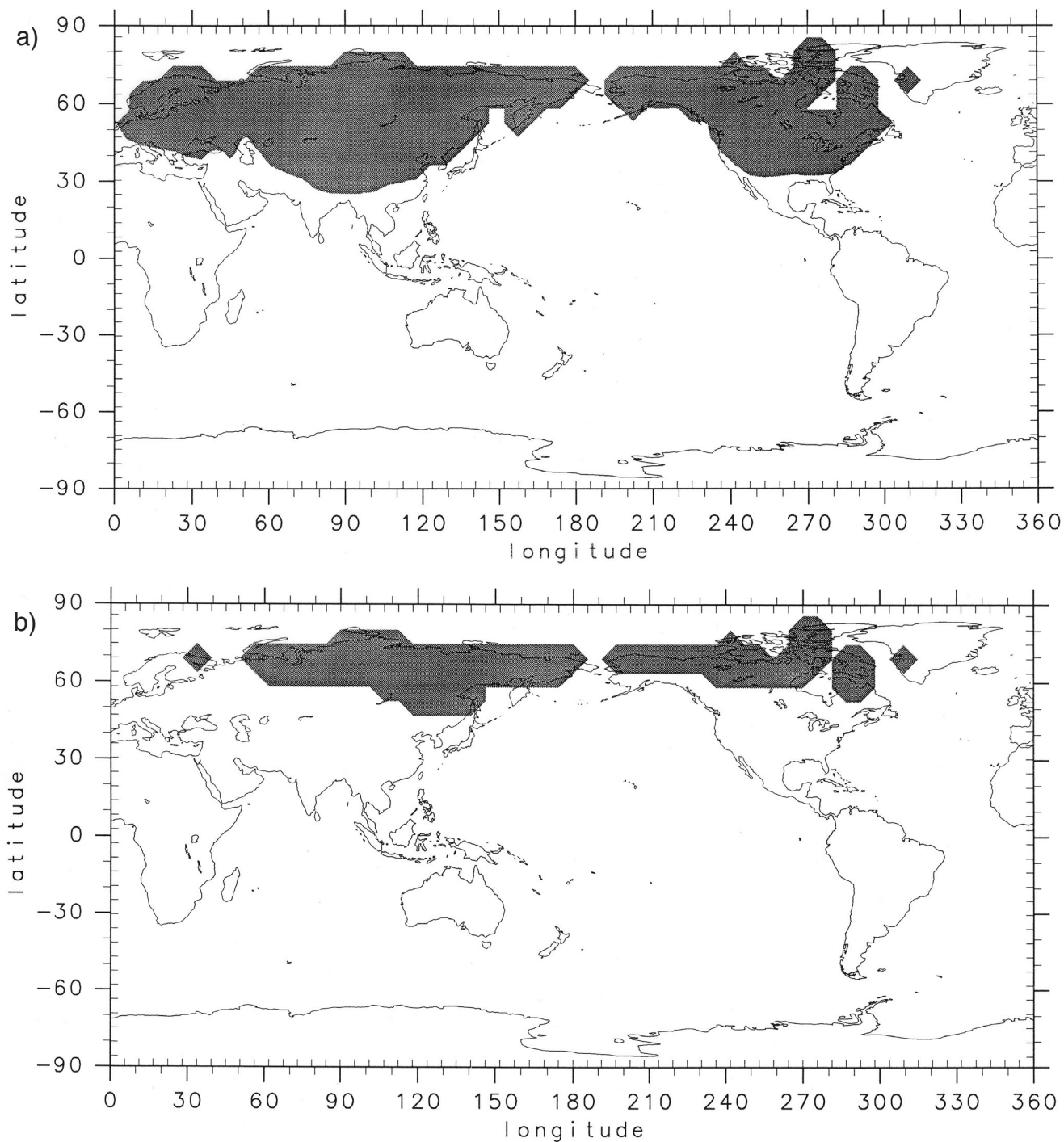


Figure 1(a) Calculated distributions of seasonally frozen ground, defined as the regions where the annual maximum of $q_i/(q_i+q_w)$ in the uppermost layer is greater than 1 for 10 day mean.
 (b) As in (a) but for permafrost, defined as the regions where the annual minimum of $q_i/(q_i+q_w)$ in the bottom layer is greater than 0.

which is very similar to that compiled from the observations (e.g., Dostovalov and Kudryavtsev, 1967). The calculated distribution of permafrost (Figure 1b) is defined as the regions where the annual minimum of $\theta_i/(\theta_i+\theta_w)$ in the bottom layer is positive, which is also very similar to Dostovalov and Kudryavtsev (1967).

Simulated soil moisture is validated against observed soil moisture at stations in frozen ground regions of Russia (Robock et al., 1995). Calculated soil water (liquid plus ice), $\theta_i+\theta_w$, relative to q_s is compared with the measured available soil water (liquid plus ice), $W-W_{wilt}$ (where W is measured soil water and W_{wilt} is wilting level), relative to saturated available soil water,

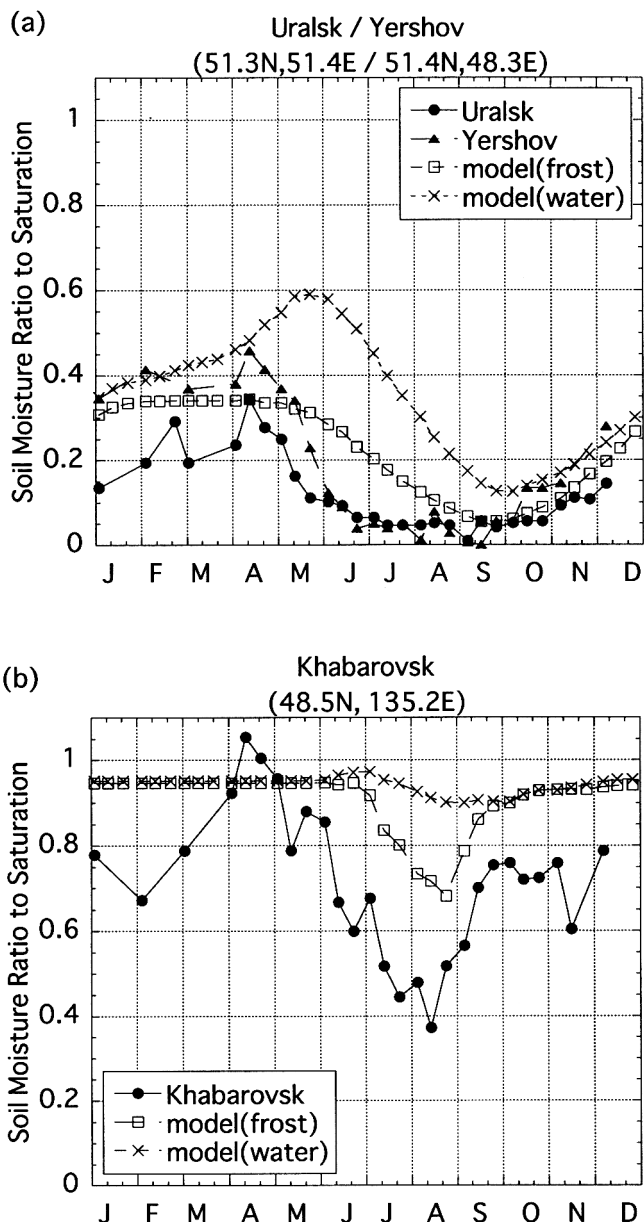


Figure 2 The ratio of observed available soil water to saturation available soil water, $(W - W_{wilt}) / (W_t - W_{wilt})$, for 0-50 cm depth (Robock et al., 1995), and calculated soil moisture to the saturation value, $(\theta_i + \theta_w) / \theta_s$, for 0-40 cm at (a) Uralsk and Yershov, and (b) Khabarovsk. Observed values (solid circle and solid triangle) are the average from 1978 to 1983, and simulated values (open square is with soil freezing, and cross is without) are the climatology of 20 years.

$W_{total} - W_{wilt}$ (where W_{total} is total water-holding capacity), since they are physically equal. Figure 2 shows the climatological seasonal cycle of $(W - W_{wilt}) / (W_{total} - W_{wilt})$ at Uralsk, Yershov and Khabarovsk, and $(\theta_i + \theta_w) / \theta_s$ at the nearest grid point of AGCM. Soil water is larger in winter than in summer, and has a maximum value in snowmelt season. The relative soil water and seasonal cycle amplitudes at the two sites are well captured by the model.

Impact of frozen ground is examined from the difference between the two runs, F-N. It is useful first to

look at impact in central Siberia (90-120°E, 40-65°N). Figure 3a shows time-height section of F-N in atmospheric and soil temperature, and Figure 3b shows the time series of F-N in surface water fluxes. A positive anomaly in soil temperature with a maximum at the bottom from winter to spring is due to the release of latent heat during freezing. The positive anomaly is reduced in magnitude towards the surface, thus the surface temperature anomaly is small during this period. There is another positive anomaly in soil temperature with a maximum at the surface in summer, which is attributed to a negative anomaly of soil moisture in the upper layers (not shown). This is consistent with negative anomalies in evaporation and precipitation in summer (Figure 3b). The smaller surface soil moisture in F run is possibly the result of a larger runoff in spring (Figure 3b) due to impermeability of frozen soil, and/or limiting evaporative (i.e., liquid) soil moisture in upper

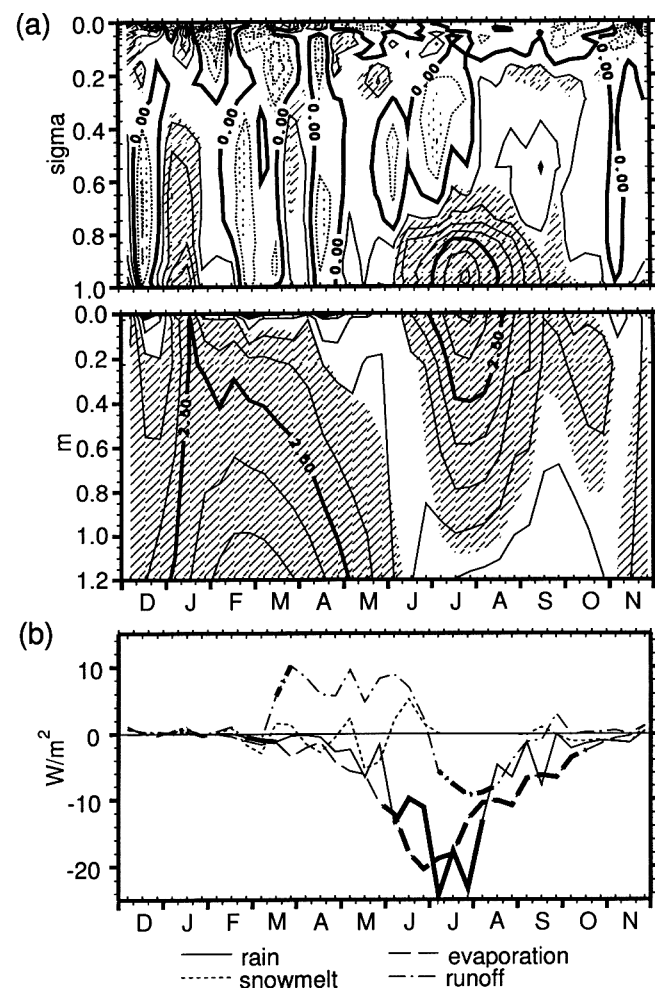


Figure 3 Difference between with and without soil freezing (F-N) in central Siberia (90-120°E, 40-65°N). (a) Time-height section of air and soil temperature (isotherm interval = 0.5K). Dotted lines denote negative values. Shadings denote statistically significant portions at a 95% confidence level. Atmospheric vertical coordinate, sigma σ , is standardized pressure coordinate by surface pressure, p/ps. (b) Time series of rainfall (solid line), evaporation (dotted line), snowmelt (dashed line) and runoff (dash-dotted line) ($1 \text{ W/m}^2 = 1.0368 \text{ mm/month}$). Thick lines denote statistically significant portions at a 95% confidence level.

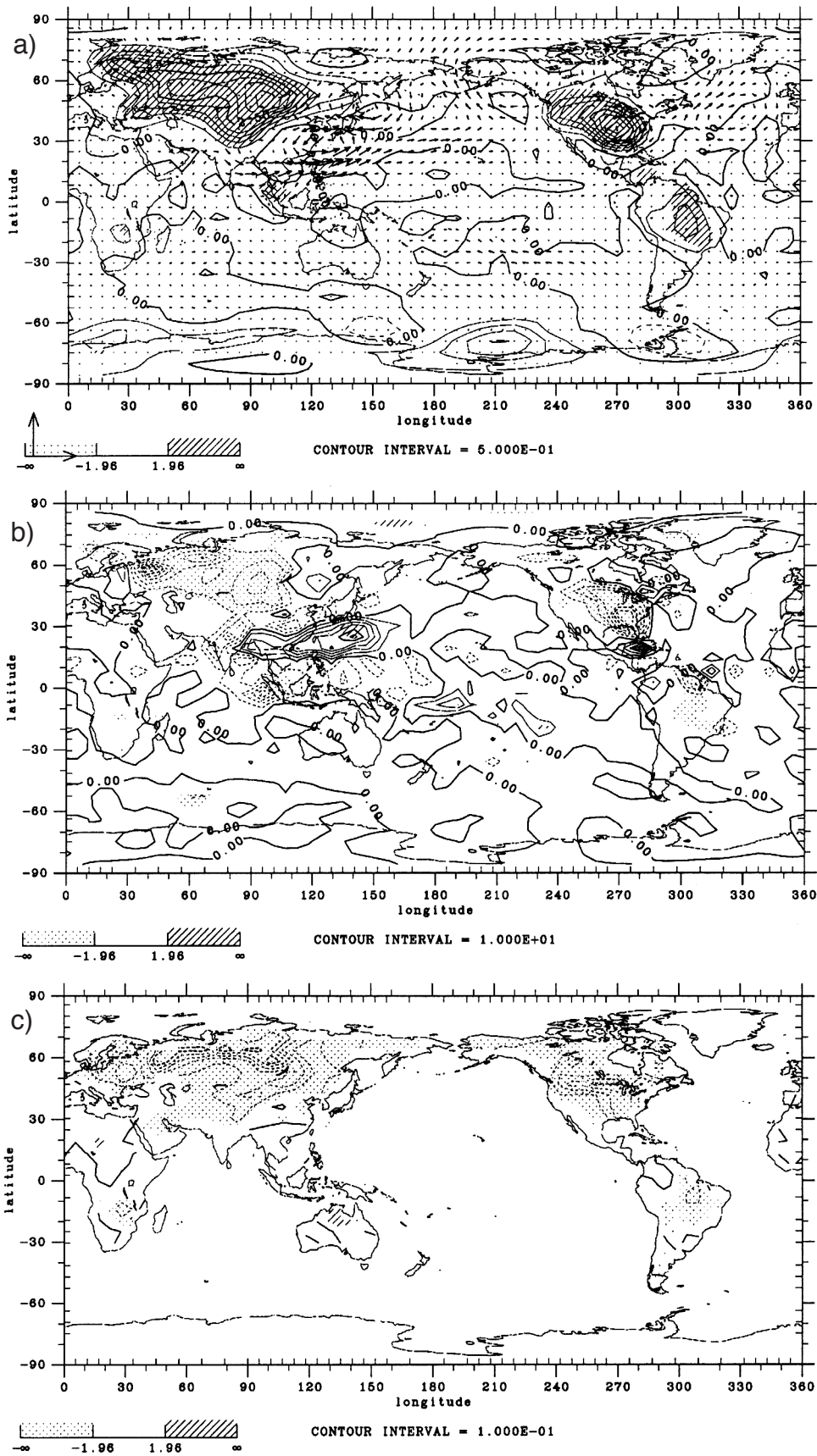


Figure 4(a) Difference (F-N) in surface air temperature (isotherm interval = 0.5K) and vertically integrated water vapor flux (unit arrow shown to the left below of the figure = $150(\text{kg}/\text{m}^2) \cdot (\text{m}/\text{s})$) in summer (average from June to August). Dashed lines denote negative values. Hatches denote statistically significant regions at a 95% confidence level.
 (b) As in (a) but for precipitation (isoline interval = $10W/m^2 = 10.4 \text{ mm/month}$).
 (c) As in (a) but for surface soil moisture ratio to the saturation (isoline interval = 0.1).

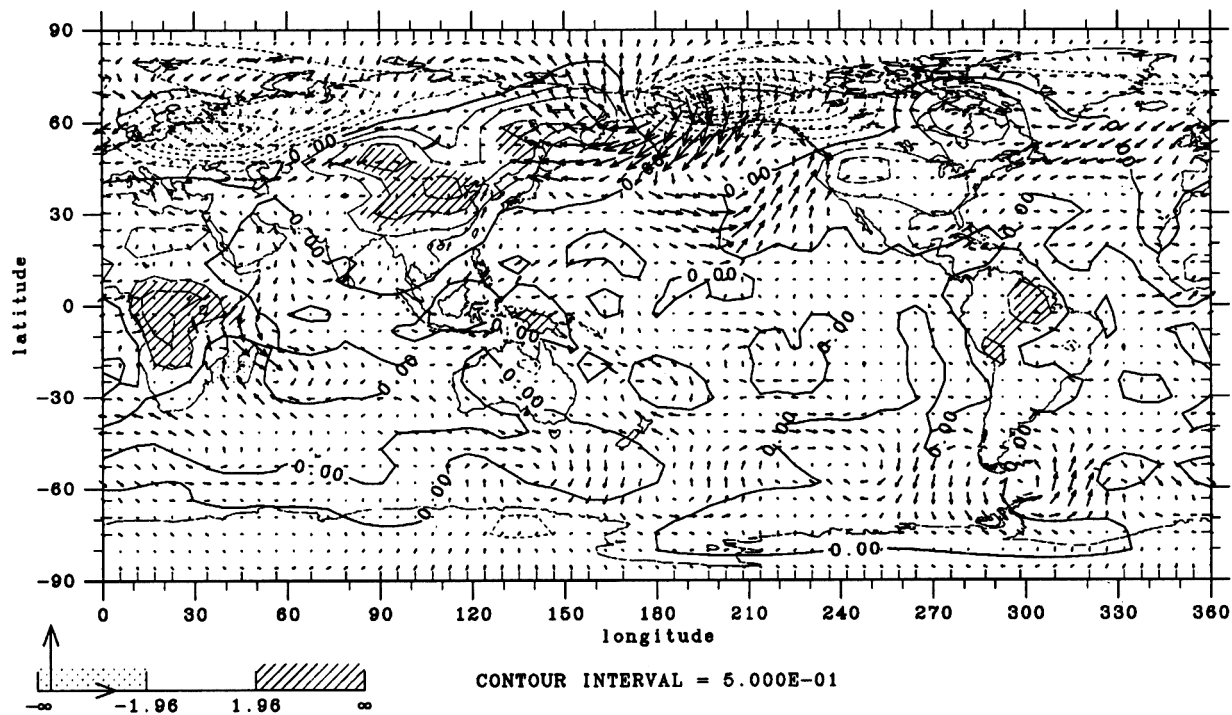


Figure 5 As in Figure 4(a) but for surface air temperature (isotherm interval = 0.5K) and surface wind (unit arrow shown to the left below of the figure = 5 m/s) in winter (average from December to February). Dashed lines denote negative values.

layers because of underlying frozen ground. This relation will be examined further below.

Let us now look at the continental-scale distribution of the impacts. Figure 4 shows F-N for (a) surface air temperature and water vapor flux, (b) precipitation and (c) surface soil moisture in summer (June to August). A large positive anomaly in surface air temperature is observed for mid to high latitude terrestrial areas (Figure 4a), which should lead to stronger summer monsoon. Associated water vapor fluxes (Figure 4a) and precipitation (Figure 4b) are larger, particularly in East Asian monsoon region where the anomaly is about 10 % of the original field. On the other hand, a negative precipitation anomaly is observed in the middle of the Eurasian and North American continents (Figure 4b). It can be explained by smaller evaporation in these regions (not shown). Location of the negative evaporation anomaly coincides with that of the positive temperature anomaly, which is consistent in view of surface water and energy budgets. Smaller evaporation could be caused by smaller surface soil moisture. In fact, surface soil moisture has a negative anomaly over the land in high latitudes (Figure 4c).

It should be noted that the moisture anomaly maximum is located in higher latitudes than that of temperature. The negative moisture anomaly is possibly caused by the larger runoff in spring induced by impermeability of frozen soil, and by the limitation of evaporative (i.e., liquid) soil moisture in upper layers because of

underlying frozen layers, as mentioned earlier. Since the thaw depth is shallower in higher latitudes, the latter should bring about the larger negative moisture anomaly in higher latitudes. In contrast, the positive temperature anomaly could be explained by larger potential evaporation in lower latitudes. If potential evaporation is large, the positive temperature anomaly would also be large even if the negative soil moisture anomaly is small, and vice versa. The distribution of potential evaporation (not shown) coincides fairly well with the distribution of the temperature anomaly. It is thus concluded that the magnitude of temperature anomaly is governed by potential evaporation and the magnitude of soil moisture anomaly by thaw depth.

In winter (from December to February), a positive anomaly in surface air temperature lies between 30-60°N over the land (Figure 5). This temperature anomaly leads to weaker cold anti-cyclones over the land, and thus a weaker winter monsoon. It is evident in the mid-latitudes to the east of the continents as a westward anomaly in surface wind (Figure 5). This surface wind anomaly leads to smaller evaporation over the ocean in these regions (not shown).

It is mentioned above that the large positive anomaly in soil temperature in winter is due to release of latent heat for freezing. If the latent heat played a major role in the development of the positive surface temperature anomaly, the anomaly should appear over all of the frozen ground regions. However, the positive anomaly

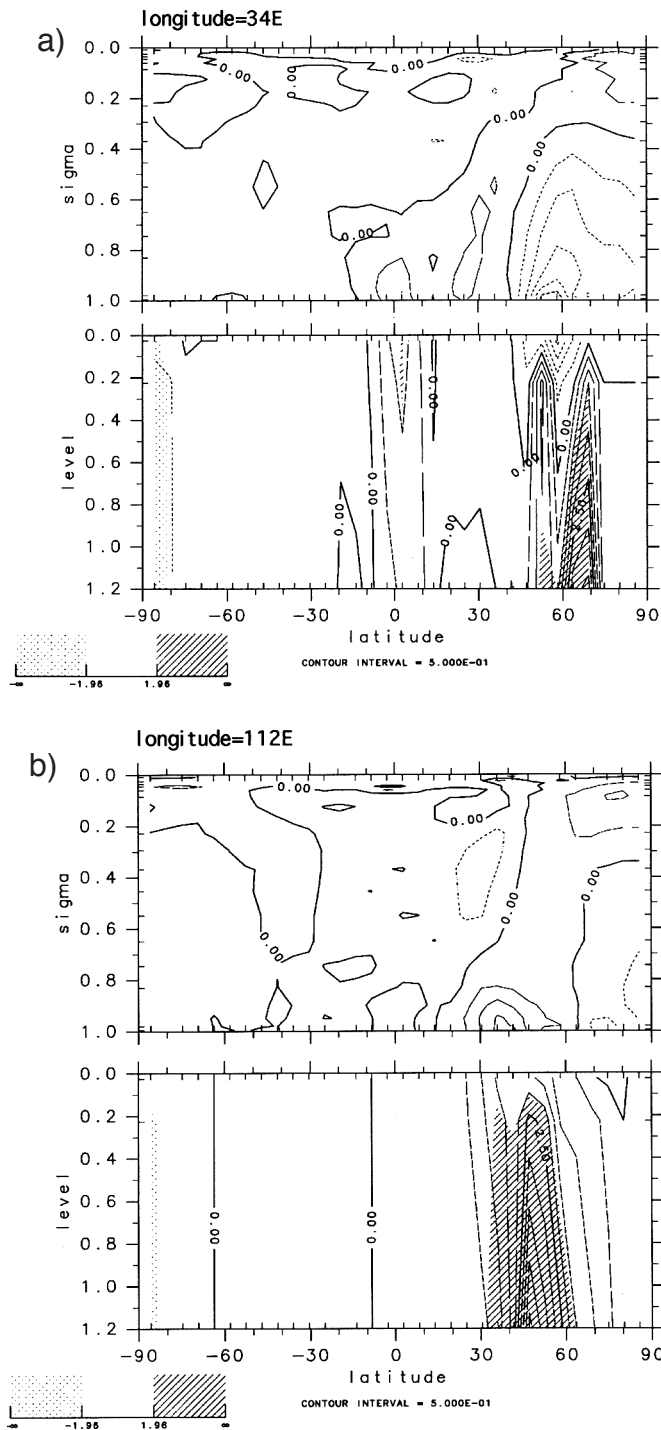


Figure 6(a) Latitude-height section of the difference (F-N) in air and soil temperature at 34°E (isotherm interval = 0.5K). Dashed lines denote negative values. Hatches denote statistically significant portions at a 95% confidence level.
 (b) As in (a) but for 112°E.

appears only in the eastern part of the continents, and the anomaly is negative in the western part. This contrast between east and west is explained by the combination of the atmosphere and soil temperature anomalies. Figure 6 shows a latitude-height section of the atmospheric and soil temperature anomaly along 34°E and 112°E. A positive soil temperature anomaly is

observed in the latitudes corresponding to frozen ground regions of both longitudinal sections. However, the positive soil temperature anomaly seems to be negated by the atmospheric anomaly in the 34°E cross section (Figure 6a), while it is coupled to the atmospheric anomaly in the 112°E cross section (Figure 6b). The surface air temperature anomaly is, therefore, more likely to be governed by dynamical variations of the atmosphere than changes in surface processes.

Concluding remarks

The global climatic impact of the freezing and melting of soil moisture was studied in terms of the interactions between the atmosphere and the ground surface. The CCSR/NIES AGCM with a multi-layer soil model was used with the seasonal-varying climatological sea surface temperature. Although the soil model used in this study is quite simple, simulated seasonal cycle of soil moisture is validated favorably against observations at several stations in permafrost regions of Russia.

It was found that inclusion of the freezing process leads to higher surface temperature in mid to high latitudes over the land in summer. This is related to a negative surface soil moisture anomaly and the potential evaporation field. The smaller surface soil moisture is caused by less evaporative (i.e., liquid) soil water due to underlying frozen ground, and by the larger runoff in spring due to impermeability of frozen soil. The positive temperature anomalies lead to larger water vapor fluxes and precipitation associated with stronger summer monsoons. In winter, frozen ground regions may have a potential to develop a positive surface air temperature anomaly due to latent heat release of freezing. A positive temperature anomaly and weaker winter monsoons are observed in the eastern part of the continents. However, the surface air temperature anomaly is more likely to be governed by dynamical variations of the atmosphere than changes in surface processes.

The climatic effects of frozen ground are, therefore, found not only in high latitudes but also in lower latitudes. The magnitude of the impact may be different according to the modeling methods, parameters or resolution of the soil model. Further investigation is needed of how sensitive the magnitude of the response is to the formulation of the soil model.

References

- Arakawa, A. and Schubert, W.H.** (1974). Interactions of cumulus cloud ensemble with the large-scale environment. Part I. *Journal of Atmospheric Science*, **31**, 671-701.
- Delworth, T. and Manabe, S.** (1989). The influence of soil wetness on near-surface atmospheric variability. *Journal of Climate*, **2**, 1447-1462.
- Dostovalov, B.N. and Kudryavtsev, V.A.** (1967). General theory of frozen ground. Moscow University Press (in Russian).
- Le Treut, H. and Li, Z.-X.** (1991). Sensitivity of an atmospheric general circulation model to prescribed SST changes: feedback effects associated with the simulation of cloud optical properties. *Climate Dynamics*, **5**, 175-187.
- Louis, J.** (1979). A parametric model of vertical eddy fluxes in the atmosphere. *Boundary Layer Meteorology*, **17**, 187-202.
- Manabe, S.** (1969). Climate and the ocean circulation, 1. The atmospheric circulation and the hydrology of the earth's surface. *Monthly Weather Review*, **97**, 739-805.
- McFarlane, N.A.** (1987). The effect of orographically excited wave drag on the general circulation of the lower stratosphere and troposphere. *Journal of Atmospheric Research*, **44**, 1775-1800.
- Mellor, G.L. and Yamada, T.** (1982). Development of a turbulence closure model for geophysical fluid problems. *Review of Geophysical and Space Physics*, **20**, 851-875.
- Nakajima, T., Tsukamoto, M., Tsushima, Y. and Numaguti, A.** (1995). Modeling of the radiative process in a AGCM. In *Climate System Dynamics and Modeling*. Center for Climate System Research, University of Tokyo, Tokyo, pp. 104-123.
- Numaguti, A., Takahashi, M., Nakajima, T. and Sumi, A.** (1995). Description of CCSR/NIES Atmospheric General Circulation Model. In *Climate System Dynamics and Modeling*. Center for Climate System Research, University of Tokyo, Tokyo, pp. 1-27.
- Robock, A., Vinnikov, K.Y., Schlosser, C.A., Speranskaya, N.A., and Xue, Y.** (1995). Use of middle latitudes soil moisture and meteorological observations to validate soil moisture simulation with biosphere and bucket models. *Journal of Climate*, **8**, 15-35.
- Romanovsky, V.E. and Osterkamp, T.E.** (1995). Interannual variations of the thermal regime of the active layer and near-surface permafrost in northern Alaska. *Permafrost and Periglacial Processes*, **6**, 313-335.
- Waelbroeck, C.** (1993). Climate-soil processes in the presence of permafrost: a system modeling approach. *Ecological Modeling*, **69**, 185-225.